Separation Science and Technology
Publication details, including instructions for authors and subscription information:
http://www.informaworld.com/smpp/title~content=t713708471

Applicability of the Perturbed Hard Chain Equation of State for Simulation of Distillation Processes in the Oleochemical Industry. Part I: Separation of Fatty Acids

G. Aly[a]; I. Ashour[a]
[a] DEPARTMENT OF CHEMICAL ENGINEERING I, LUND UNIVERSITY, LUND, SWEDEN

To cite this Article Aly, G. and Ashour, I.(1992) 'Applicability of the Perturbed Hard Chain Equation of State for Simulation of Distillation Processes in the Oleochemical Industry. Part I: Separation of Fatty Acids', Separation Science and Technology, 27: 7, 955 — 974
To link to this Article: DOI: 10.1080/01496399208019735
URL: http://dx.doi.org/10.1080/01496399208019735

SEPARATION SCIENCE AND TECHNOLOGY, 27(7), pp. 955–974, 1992

Applicability of the Perturbed Hard Chain Equation of State for Simulation of Distillation Processes in the Oleochemical Industry. Part I: Separation of Fatty Acids*

G. ALY and I. ASHOUR
DEPARTMENT OF CHEMICAL ENGINEERING I
LUND UNIVERSITY
P.O. BOX 124, S-221 00 LUND, SWEDEN

Abstract

Fatty acids constitute an important group of chemicals with extensive end-use markets, either for their direct uses or for the intermediate uses of their numerous derivatives. These oleochemical products are currently purified or fractionated using distillation at subatomspheric pressures. Due to the increasing interest of the pharmaceutical industry in some fatty acids with high purity, supercritical fluid extraction followed by appropriate fractionation steps are also employed. It would therefore be convenient to utilize a single thermodynamic model that is capable of predicting all thermodynamic properties needed, and covering the whole pressure range which is currently applied in both industries. Different equations of state and activity coefficient models were scanned, and the perturbed hard chain equation of state (PHC-EOS) provided results which are as good as those obtained using activity coefficient models, and in some cases better. Since there are very scarce experimental data on the behavior of binary mixtures containing species with associative tendency, an attempt was also made to incorporate a correlation for the dimerization constants to account for chemical association of these higher carboxylic acids. Using a comprehensive and thermodynamically screened vapor pressure data base, pure component parameters for the C_6–C_{20} fatty acids were computed. The fitted parameters were incorporated in the PHC-EOS and resulted in good reproduction of binary vapor–liquid equilibria. Calculations of multicomponent mixtures were performed using these binary parameters. A flow-sheeting program was utilized to simulate a distillation process consisting of two integrated columns, operated at subatmospheric pressures, for the purification of different hydrogenated fatty acid feedstocks. The simulated flow rate, concentration, and temperature profiles were compared with some real operating data obtained from a major oleochemical plant. Analysis of this comparison revealed that the PHC-EOS is

*Dedicated to Prof. Å. Jernqvist on the occasion of his 60th birthday.

very well suited for simulating different distillation processes for the purification and fractionation of C_6–C_{20} fatty acids. Furthermore, the need for more accurate thermodynamic information describing the chemical association of these compounds was also accentuated.

INTRODUCTION

Oleochemical products constitute a significant part of the chemical industry and the advanced industrial economy. They may be classified as fatty acids, fatty alcohols, fatty acid methyl esters, fatty amines, and glycerine. The end-use markets of these products are extensive for either their direct uses or for the intermediate uses of their numerous derivatives. The raw materials for most natural oleochemicals are animal fats, such as inedible tallow and grease, and vegetable oils, such as palm oil, palm kernel oil, coconut oil, soybean oil, sunflower oil, rapeseed oil, and others. The third major source is crude tall oil which is a by-product of the kraft pulping process.

World production of fats and oils in 1990 has been estimated to 80.6 Mton, and is projected to reach 105 Mton by the year 2000 (*1*). Palm oil and palm kernel oil are steadily displacing tallow and coconut oil, respectively, due to the rapid increase of mature oil palm areas. According to the same source, world production of natural fatty acids in 1988 was 2.23 Mton and is projected to increase at an average annual rate of 2.1% to reach 2.86 Mton by the year 2000. These figures do not include synthetic fatty acids, originating from petrochemical feedstocks, or tall oil fatty acids.

The initial process for obtaining fatty acids from fats and oils is hydrolysis, whereas the triglycerides are split, by means of water, into diluted glycerine solution and mixed fatty acids with linear even-numbered carbon chains. This mixture is purified by hydrogenation and distillation, or via separation into individual fatty acids of different chain lengths by fractional distillation. Mixed fatty acids can also be separated by recrystallization from either an organic solvent or from an aqueous surfactant solution.

In this investigation, particular attention has been devoted to low pressure distillation processes operated in the oleochemical industry. Multicomponent fatty acid mixtures containing water have been considered. Equations of state and activity coefficient models were compared to select a reliable thermodynamic model which can be used in simulating these processes.

PROCESSING OF INDUSTRIAL FATTY ACIDS

Figure 1 displays a simplified block diagram for the industrial processing of fatty acids. Generally, the first processing step involves acid pretreatment to remove phosphatides, followed by water washing to remove the

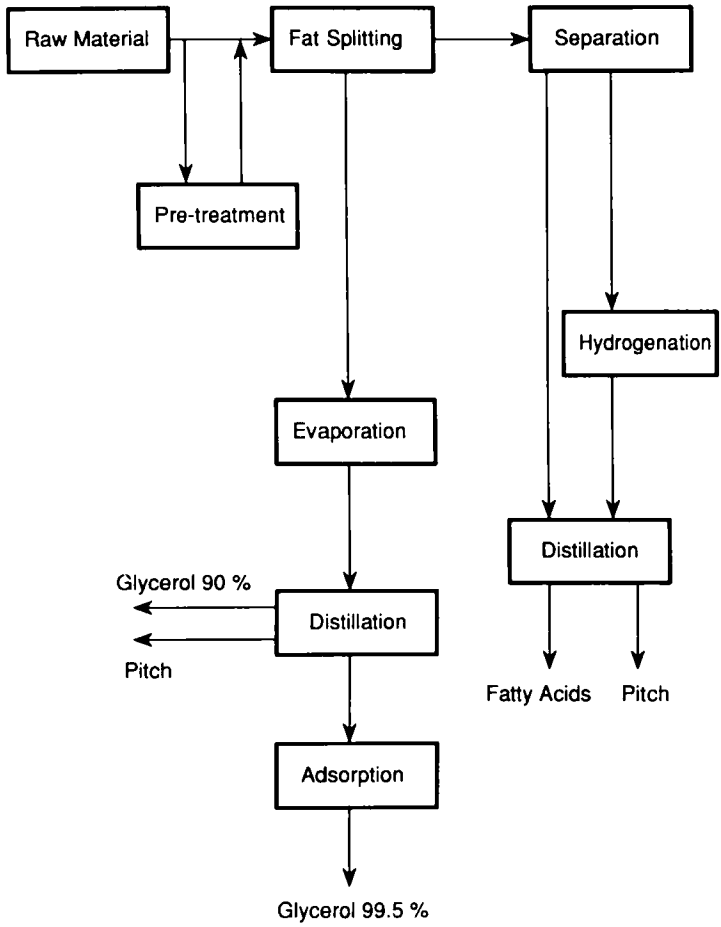

FIG. 1. Block diagram for general processing of fatty acids.

residual acid. The next step is hydrolysis of the pretreated fats to split the triglyceride into a diluted aqueous glycerine solution and a mixture of different fatty acids.

The hydrolysis reaction is usually carried out continuously using deionized and deaerated water at a temperature of 250–255°C and a pressure of 50–55 bar. The high temperature and pressure employed assures a higher water solubility in the fat phase, but the use of high pressure is primarily to keep water in the liquid phase at temperatures above its boiling point. Injection of direct high-pressure steam in the hydrolysis reactor is frequently practiced to retain the reaction temperature and increase the ag-

itation intensity of the reacting phases. High overall efficiencies, with conversions in excess of 99%, are usually attained in this continuous and countercurrent hydrolysis step. This is attributed to the fact that water is used both as a reactant (hydrolysis water) and as a by-product remover (excess water). During hydrolysis, the water stream percolates down through the ascending fat phase in a finely divided form and almost completely removes the liberated glycerol. Enzymatic hydrolysis of triglycerides is a more recent process development. The process operates at ambient temperatures and atmospheric pressure. However, the enzymes used are expensive and require much longer reaction times compared to conventional hydrolysis.

The glycerine obtained from the hydrolysis, usually known as sweetwater, contains 8–12 wt% glycerol, together with varying amounts of dissolved inorganic salts and color and fat impurities. This stream is processed through multiple-effect evaporation to a concentration of 88 wt%, followed by distillation to a purity exceeding 99.5 wt%. The distilled product is finally treated by active carbon adsorption to increase its color stability. A by-product stream containing 90 wt% glycerol is also obtained from the distillation step, and it can either be redistilled or sold as such.

Crude fatty acids emerging from the fat splitter are usually processed into purer products using hydrogenation and distillation. The main goal of the hydrogenation step is to lower the iodine value, which is a measure of the amount of unsaturation, by saturating the ethylenic linkage in the fatty acid chain to produce a more saturated acid. A catalyst such as nickel, palladium, or platinum is utilized, with nickel being the most common catalyst used in the oleochemical industry. The operating conditions of the catalytic hydrogenation process vary depending on the type of fatty acid, its purity, degree of saturation required, and the overall process configuration. Most of the commercial reactors used in this step are operated at pressures of 20–34 bar, temperatures of 120–260°C, and nickel catalyst concentration of 0.06–1.0% (*2*).

The hydrogenated fatty acid feedstocks are usually refined using distillation to remove odor and color-causing low-boiling components, such as hydrocarbons, ketones, and aldehydes, and high-boiling components, such as polymerization products, residual triglycerides, and traces of nickel catalyst. Individual fatty acids with purities in excess of 99% can be readily produced using fractional distillation in multicolumn configurations (*3*).

Prior to distillation, the crude fatty acid feedstock is usually preheated and pumped to a vacuum dryer-deaerator, where air and most of the water content are removed. The configuration of the distillation process depends on the raw materials and the required specification of the final product. Figure 2 shows a simplified flow sheet for a fatty acid distillation process. The first column is used to fractionate out most of the low-boiling com-

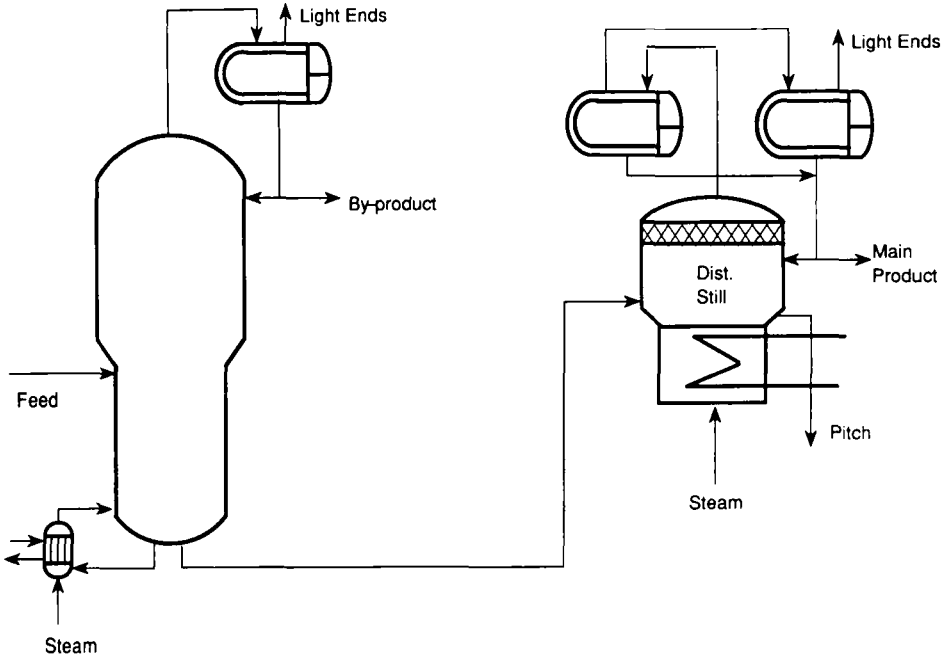

FIG. 2. Flow sheet of a distillation process for multicomponent fatty acid feedstocks.

ponents (light ends). The vapor stream passes through a partial condenser where the light ends are evacuated and lower fatty acids are condensed (by-product). This by-product stream can either be redistilled or blended with other cuts to produce salable fatty acid products. The bottom stream, consisting of higher fatty acids and high-boiling components, is fed into the second column, usually a distillation still, to separate the fatty acids (main product) from the high-boiling components (pitch). The vapor stream leaving the demister of the still contains fatty acid mixture and light ends. It is easy to separate the former fraction from the light ends by virtue of the wide spread in relative vapor pressures. This is accomplished by passing the vapors through two partial condensers, each operated at a controlled temperature, where the remaining light ends are released as vapor. Both vapor streams containing the light ends are withdrawn to the vacuum system, where they are finally condensed, and the noncondensable gases are released to the atmosphere.

To minimize the risk for chemical decomposition of the fatty acids, both columns are operated under vacuum, typically between 5 and 80 mbar. Furthermore, direct steam is injected in the reboilers to suppress the bubble point of the mixture, especially in the lower parts of both columns.

Three different processing routes are currently used for the production

of distilled hydrogenated fatty acids. The first route resembles that shown in Fig. 1, and results in products with good color stability, but the amount of nickel catalyst consumed is rather high. This aspect can create environmental problems related to the disposal of the residual pitch. The second route involves distillation followed by hydrogenation, and produces fatty acids with a high nickel content in the form of soluble nickel salts. An additional refining step must therefore be incorporated to remove nickel using sequestering agents, such as citric acid or phosphoric acid, followed by filtration. Incomplete removal of nickel after hydrogenation has an adverse effect upon color stability of distilled fatty acids. However, distillation of fatty acids prior to hydrogenation has the advantage of removing impurities so that only fatty acids are present to be hydrogenated, which greatly reduces catalyst poisoning. The third route has the sequence distillation–hydrogenation–distillation, where the second distillation step removes the residual nickel in the final product. This route is considered the best, but the production cost is much higher compared to the other routes. Besides, the overall distillation capacity of the plant is reduced.

The type and quality of raw materials, product specifications, and process economics are the main factors to be considered on deciding which of the alternative routes is to be chosen for the processing of fatty acids.

THERMODYNAMIC MODELING

In process simulation there is a need for reliable models that generate thermodynamic properties, especially phase equilibrium data. The two main thermodynamic models are activity coefficient models, usually called dual models, and equations of state (EOS). At low pressures, especially for systems containing polar and associating compounds, the dual models are employed for the liquid phase where strong nonidealities exist, while EOS are used for the gas phase. Although dual models are easy to use, they are only useful for those mixtures where all components are at subcritical pressures. Furthermore, two to four parameters per binary are required in these models, a characteristic that can lead to errors when extrapolating experimental data.

At high pressures, one would encounter difficulties resulting from the choice of the standard state, prohibiting the use of dual models. Thus, EOS are the most appropriate models for the prediction of thermodynamic properties. Comprehensive literature surveys covering EOS with their merits and limitations, for the calculation of high pressure phase equilibria, can be found in Refs. *4–6*.

During the last decade, new attempts were made to extend the applicability of cubic EOS (*7–15*) and the perturbed hard sphere equation of

state (PHS-EOS) to low pressures (*16*). These efforts were focused on modifying the PHS-EOS and the four main cubic EOS: the original van der Waals, Peng–Robinson (*17*), Redlich–Kwong–Soave (*18*), and a new virial-like equation (*15*), by using new temperature-dependent equations for the attraction parameter of the pure components. Generally, the new modified equations improved the calculations of some thermodynamic properties, such as vapor pressures and heats of vaporization. The cubic EOS were extended to binary mixtures using different types of mixing rules, and the results were compared with the dual models. These cubic EOS proved to do as well or better than the dual models for the binary systems tested, including both non-polar and polar short molecule compounds. The PHS-EOS was also extended, using the conventional mixing rule, to both binary and ternary systems including methyl chloride, dimethyl ether, and methanol. The results were compared to the UNIFAC model (*19*). The PHS-EOS resulted in accurate predictions for ternary systems based on available experimental binary information, while the UNIFAC model could not be used without defining the compounds as new groups.

The large deviation of carboxylic acids from ideal-gas behavior, even at subatmospheric pressures, is generally attributed to chemical effects, since the acid monomer undergoes partial polymerization. This association occurs in both vapor and liquid phases. If the mixture contains two carboxylic acids, the association phenomena becomes more complicated since heterodimerization between the two acids can also take place. This association drastically affects the volatility of the acids, and should be taken into account when distillation processes of their separation are being developed. There are very scarce data on the behavior of binary mixtures containing species with an associative tendency. The most probable reason behind the general lack of such data, and the inconsistencies in existing ones, is the anomalous behavior of these acids in both vapor and liquid phases, which makes experimental measurements unusually difficult. There are, however, limited studies on vapor-phase association of lower fatty acids, up to heptanoic acid (C_7), and equations for their dimerization equilibrium constants were suggested (*20*, *21*) using the "chemical theory" of gas imperfection.

The perturbed hard chain equation of state (PHC-EOS), developed by Beret and Prausnitz (*22*) for pure compounds and extended to mixtures by Donohue and Prausnitz (*23*), has been modified to include the chemical dimerization equilibria (*24*). The equation is based on an interpolation between the perturbed hard sphere theory for small molecules, which is valid for all densities, and Prigogine's theory for chain molecules, which is valid at liquidlike densities. This modification resulted in accurate prediction for small and large molecules at low and high pressures. The equa-

tion failed, however, at the critical region. Equations (1)–(8) represent the general form of the PHC-EOS.

General form:

$$Z = Z(\text{repulsive}) + Z(\text{attractive}) \tag{1}$$

where

$$Z(\text{repulsive}) = 1 + c(4\xi - 2\xi^2)/(1 - \xi)^3$$

$$Z(\text{attractive}) = \langle cT^* \rangle \sum_{m=1}^{5} \frac{m}{\tilde{v}^m}\left(\frac{A_{1m}}{T} + \frac{A_{2m}\langle T^* \rangle}{T^2}\right)$$

$$\xi = \sqrt{2}\pi/6\tilde{v}$$

$$\tilde{v} = v/v^*$$

$$\frac{z_{ij}}{z_i z_j}\frac{\phi_{ij}}{\phi_i \phi_j} = \frac{P}{P_{\text{ref}}}K_{ij} \qquad (P_{\text{ref}} = 101{,}325 \text{ N/m}^2)$$

$$\ln K_{ij} = \frac{\Delta s_{ij}}{R} - \frac{\Delta h_{ij}}{RT}$$

The mixing rules used to extend the above equation are outlined below:

$$\Delta h_{ij} = \tfrac{1}{2}(\Delta h_i + \Delta h_j) \tag{2}$$

$$c = \sum_i z_i c_i \tag{3}$$

$$v^* = \sum_i z_i v_i^* \tag{4}$$

$$\langle cT^* \rangle = \sum_i \sum_j z_i z_j (cT^* v^*)_{ij}/v^* \tag{5}$$

$$\langle T^* \rangle = \sum_i \sum_j z_i z_j (cT^{*2} v^*)_{ij} \Big/ \left(v^* \sum_i z_i c_i T_i^*\right) \tag{6}$$

$$(cT^*v^*)_{ij} = \tfrac{1}{2}(c_iT_i^*v_j^* + c_jT_j^*v_i^*)(1 - k_{ij}) \quad (7)$$

$$(cT^{*2}v^*)_{ij} = \tfrac{1}{2}(c_iT_i^{*2}v_j^* + c_jT_j^{*2}v_i^*)(1 - k_{ij}) \quad (8)$$

For pure fatty acids, the cubic EOS gave poor predictions of both vapor pressures for the pure components and phase equilibrium data for fatty acids–carbon dioxide mixtures at high pressures (*4*). On the other hand, the PHS-EOS gave good predictions for these systems at high pressures (*4*), but it could not predict the phase equilibrium data of fatty acid systems at low pressures. For the low pressure range, the dual models can be used, but they are restricted to the prediction of some thermodynamic properties. For the simulation of separation processes involved in the production of fatty acids and glycerol, it would therefore be convenient to utilize one EOS that is capable of predicting all thermodynamic properties and that covers the whole pressure range currently applied in the oleochemical industry. Accordingly, it would be possible to simulate separation processes for fatty acids and glycerol at subatmospheric pressures, including steam distillation, as well as supercritical fluid extraction of fatty acids followed by appropriate fractionation steps.

In this work the PHC-EOS has been evaluated for the prediction of vapor pressures and phase equilibrium data for fatty acids at low pressures, and the results were compared with the dual models. An attempt was also made to incorporate a correlation for the dimerization constants to account for the chemical dimerization equilibria.

SIMULATION RESULTS AND DISCUSSION

The physical properties of the most important saturated C_6–C_{20} fatty acids are given in Table 1. The critical data for C_6–C_{10} acids are experimental data (*25*), whereas those for the remaining acids were predicted (*26*). Reliable experimental data for pure component vapor pressures are needed for the development of accurate thermodynamic models. A comprehensive literature survey (*27*) resulted in the compilation of a total of 600 data points for saturated C_6–C_{20} fatty acids. The vapor pressure data were screened, and the screening procedure resulted in a data base consisting of 53.8% of the original data points. This vapor pressure data base was then used to fit Antoine constants for the different fatty acids (A_i, B_i, and C_i) in the following form of Antoine's equation:

$$\ln P^s = A + \frac{B}{T} + CT \quad (9)$$

TABLE 1
Physical Properties of Saturated C_6–C_{20} Fatty Acids

Fatty acid	Formula	mp (K)	bp (K)	T_c (K)	P_c (bar)	V_c (cm^3/mol)	ω
Caproic	$C_6H_{12}O_2$	271.50	479.0	663.0	32.0	395.0	0.608
Caprylic	$C_8H_{16}O_2$	289.66	512.7	694.0	27.0	505.0	0.754
Capric	$C_{10}H_{20}O_2$	304.55	542.7	726.0	21.0	615.0	0.854
Lauric	$C_{12}H_{24}O_2$	316.98	571.4	733.5	19.1	725.0	0.934
Myristic	$C_{14}H_{28}O_2$	327.32	599.0	755.4	16.8	835.0	1.018
Palmitic	$C_{16}H_{32}O_2$	335.66	622.3	774.2	14.3	945.0	1.027
Stearic	$C_{18}H_{36}O_2$	342.49	648.1	801.4	13.6	1055.0	1.079
Archidic	$C_{20}H_{40}O_2$	348.50	670.2	821.5	12.2	1165.0	1.100

where P^s is the vapor pressure of pure component, Pa, and T is the corresponding temperature, K. The results of parameter fitting are displayed in Table 2, together with the valid temperature ranges and the average relative deviation, σ_{pav}. Except for archidic acid, the deviation is in the range 0.85–3.02%, and it may therefore be concluded that the screened vapor pressure data base for the saturated C_6–C_{18} fatty acids can be considered as reliable across a wide range of temperature. The parameter fitting procedure for archidic acid was somewhat different. Measured at relatively higher temperatures, the experimental vapor pressure data were first fitted to the Abrams–Prausnitz correlation (*28*) which is frequently used for extrapolation of vapor pressures to lower temperatures. The extrapolated vapor pressure data were then fitted to Antoine's equation to determine A, B, and C for archidic acid at low temperatures. This procedure resulted in an average relative deviation of 15.9%, which is normally accepted for such higher compounds.

TABLE 2
Fitted Antoine Constants for Saturated C_6–C_{20} Fatty Acids

Fatty acid	Temperature range (K)	A	$-B$	$-C$	σ_{pav}
Caproic (C_6)	272.15–504.15	36.74529	9318.28	0.01202750	0.93
Caprylic (C_8)	295.74–540.15	39.33114	10598.33	0.01392670	0.85
Capric (C_{10})	307.49–572.15	41.81431	11865.32	0.01553655	0.95
Lauric (C_{12})	325.31–603.15	43.56900	12904.24	0.01656523	3.02
Myristic (C_{14})	335.64–596.85	46.80553	14294.41	0.01908606	1.70
Palmitic (C_{16})	350.79–604.45	49.11704	15488.41	0.02049479	1.15
Stearic (C_{18})	365.58–627.55	51.26976	16615.03	0.02186564	2.70
Archidic (C_{20})	360.15–670.15	45.15758	15496.39	0.01566631	15.90

The Tsonopoulos–Prausnitz equation for the dimerization equilibrium constants was used (*20*). The pure component parameters T_i^*, v_i^*, and the Prigogine factor c_i were fitted using the screened vapor pressure data base, with and without dimerization equilibria. The weighted least square method and an appropriate objective function were applied in these computations. The PHC-EOS prediction of vapor pressures using dimerization equilibria is illustrated for caproic acid in Fig. 3, where the average relative deviation, σ_{pav}, is plotted against temperature. The results of the computations without taking dimerization equilibria into consideration are also plotted for comparison. As can be seen, the difference between both cases is remarkably small. This can be attributed to two main reasons. First, the Tsonopoulos–Prausnitz equation for the dimerization equilibrium constants, although derived for lower carboxylic acids, was assumed to be valid for all acids, an assumption that seems to be unacceptable. Second, it is most probable that trimers and even higher association products are also formed, a factor which was neglected in this work due to the general lack of published data. The need for accurate experimental data is perhaps nowhere more apparent than with fatty acids. Their importance in both chemical and oleochemical

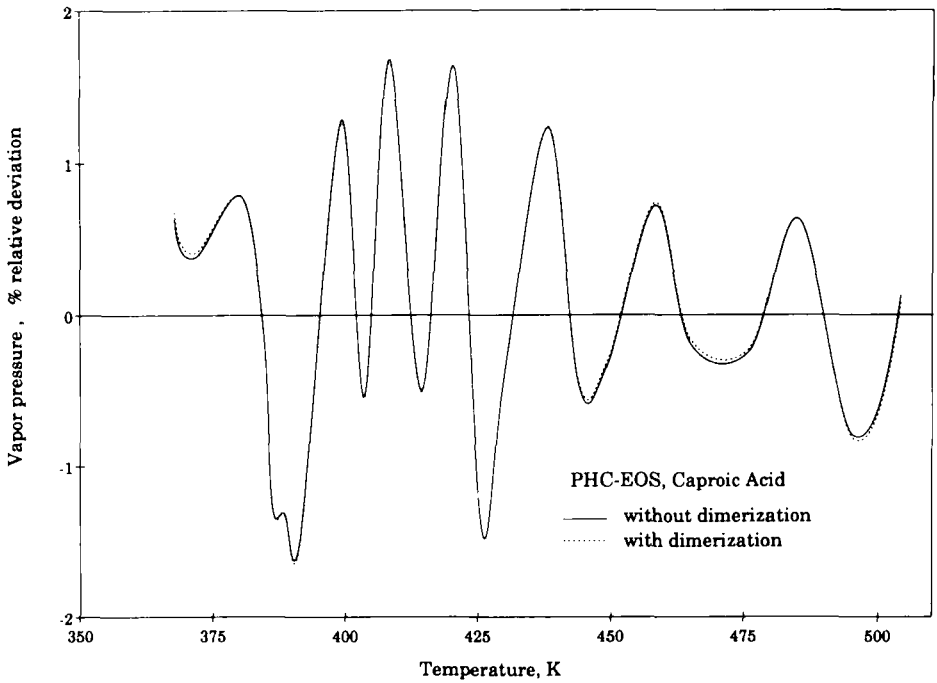

FIG. 3. Relative deviation of the PHC-EOS vapor pressure prediction for caproic acid.

industries, together with their associative behavior in both vapor and liquid phases, accentuate the need for these data. The computations with dimerization equilibria failed to converge for the other fatty acids, C_8–C_{20}, and it was decided to neglect the association behavior in further calculations.

Table 3 shows the pure component parameters T_i^*, v_i^*, and c_i together with the resulting deviations, σ_p, minimum vapor pressure, and temperature ranges. These results reflect the performance of the PHC-EOS for vapor pressure predictions without taking the dimerization equilibria into consideration. As can be seen, σ_{pav} is in the range 0.13–0.79% whereas the maximum deviation, σ_{pmax}, is in the range 0.89–1.71%, except for stearic acid, where it reached a value of 8.19%. Again, the high relative deviations for archidic acid can be attributed to the quality of the extrapolated vapor pressure data mentioned earlier. It should be realized that cubic equations of state would yield maximum deviations up to 60% for most C_6–C_{20} fatty acids and would certainly fail for some others (*4*). When dealing with equations of state for phase equilibrium calculations, it is important that the equation accurately represents the properties of pure components in the saturation region with a special emphasis on vapor pressure.

The binary interaction parameters to be used in the PHC-EOS, k_{ij}, were fitted to vapor–liquid equilibrium (VLE) data for binary fatty acid mixtures. In this work the k_{ij} characterizing the physical interactions between two different molecules were considered to be temperature-independent. The results of these computations are given in Table 4 for six binary fatty acid systems. The table shows the binary interaction parameters for PHC-EOS, k_{ij}, pressure and pressure range, average and maximum deviations of pressure, and liquid- and vapor-phase composition. The prediction of

TABLE 3
Pure Component Parameters for Saturated C_6–C_{20} Fatty Acids

Fatty acid	Temperature (K)	P (minimum) (Pa)	T^* (K)	100 v^* (dm³/mol)	c	σ_{pav}	σ_{pmax}
Caproic	367.75–504.15	1066.57	349.0550	7.087279	4.04054	0.787	1.636
Caprylic	371.05–540.15	266.64	319.4053	17.65199	5.364454	0.197	−0.893
Capric	375.55–527.15	79.99	327.7394	21.14771	5.768438	0.27	0.963
Lauric	380.05–529.15	26.66	331.3798	27.66482	6.243813	0.46	−0.982
Myristic	357.72–553.65	1.00	330.7266	39.80364	6.831590	0.71	−1.709
Palmitic	371.21–557.35	0.80	338.2693	43.7062	7.141142	0.51	−1.048
Stearic	365.58–564.15	0.10	337.1369	59.48127	7.760232	0.13	8.187
Archidic	360.15–583.15	0.08	639.4309	1.081766	2.899333	15.80	−52.01
Water	273.15–643.15	610.40	310.6613	3.653181	3.069031	0.31	−5.34

TABLE 4
Binary Interaction Parameters for Saturated C_6–C_{20} Fatty Acids

Component	Pressure (bar)	k_{12}	Pressure		Liquid mole fraction		Vapor mole fraction	
			σ_{pav}	σ_{pmax}	σ_{xav}	σ_{xmax}	σ_{yav}	σ_{ymax}
Caproic (1)	0.013	5.9104 E-3	0.87	2.33	0.015	−0.05	2.76	7.95
Caprylic (2)	0.04	9.5662 E-3	1.62	−2.43	0.010	−0.03	2.14	4.18
	0.067	1.2161 E-2	1.49	3.97	0.013	0.04	1.26	−4.80
	0.133	1.1901 E-2	1.29	2.47	0.017	0.05	2.06	−5.81
	0.013–0.133	9.7479 E-3	2.03	4.49	0.018	0.08	2.26	−8.69
Caprylic (1)	0.005	−5.9884 E-3	3.01	7.17	0.013	0.02	2.96	4.37
Capric (2)	0.027	−2.4281 E-3	1.21	2.24	0.009	−0.02	1.13	2.05
	0.133	−7.8429 E-4	2.34	3.35	0.018	0.09	1.77	1.97
	0.005–0.133	−3.5380 E-3	2.41	9.46	0.020	0.08	2.45	9.87
Capric (1)	0.005	−1.4998 E-3	6.29	−8.14	0.039	−0.07	4.41	9.20
Lauric (2)	0.133	2.2466 E-3	1.12	−2.37	0.010	−0.02	0.89	3.55
	0.005–0.133	8.0395 E-3	8.07	−13.32	0.067	−0.09	5.34	−18.83
Lauric (1)	0.044	−8.1195 E-4	7.87	−11.56	0.037	−0.12	4.82	16.51
Myristic (2)	0.013	−3.0307 E-4	1.22	−3.30	0.010	−0.02	1.63	4.47
	0.067	3.0058 E-3	0.96	−1.75	0.012	0.24	1.35	2.93
	0.004–0.067	2.7818 E-4	3.54	−10.77	0.026	−0.15	3.28	19.71
Myristic (1)	0.004	2.6763 E-3	4.28	−7.45	0.029	−0.11	2.53	15.46
Palmitic (2)	0.005	−6.9933 E-3	2.21	7.87	0.044	−0.06	4.01	7.69
	0.013	3.6242 E-4	0.88	2.03	0.011	−0.04	1.79	5.49
	0.067	1.7880 E-3	0.82	1.84	0.015	0.03	2.45	−6.43
	0.004–0.067	−9.1102 E-4	3.71	−10.51	0.043	−0.21	4.17	24.88
Palmitic (1)	0.005	−6.6366 E-3	2.17	−3.36	0.027	0.06	3.11	−7.19
Stearic (2)	0.007	9.6036 E-3	16.73	−30.09	0.089	−0.18	9.83	26.41
	0.005–0.007	1.0688 E-3	13.57	−27.10	0.099	−0.27	6.81	31.92

VLE is generally good but the relative deviation in the composition of the vapor phase is much higher than in the liquid phase and seems to increase with higher carbon numbers. This may be attributed to neglecting the dimerization equilibria as explained earlier.

The performance of the PHC-EOS in predicting VLE was compared to that obtained using five different dual models. The results are depicted in Table 5 for the six systems, and in Fig. 4 for the myristic acid–palmitic acid binary system at 4 mbar. The activity coefficients were taken from Gmehling et al. (*29*) and the simulations were performed using EQUIL

TABLE 5
Comparison of VLE Predictions by PHC-EOS and Dual Models

Component	Pressure (bar)	PHC-EOS				Activity coefficient model				
		ΔT_{av}	ΔT_{max}	Δy_{av}	Δy_{max}	ΔT_{av}	ΔT_{max}	Δy_{av}	Δy_{max}	Model[a]
Caproic (1)	0.013	0.044	−0.128	0.019	0.044	0.39	0.88	0.017	0.060	a
Caprylic (2)	0.133	0.050	−0.096	0.011	0.022	0.21	0.51	0.003	0.009	b
Caprylic (1)	0.005	0.178	−0.407	0.017	0.032	1.11	2.67	0.019	0.032	c
Capric (2)	0.133	0.091	0.574	0.014	−0.095	0.28	0.92	0.004	0.011	d
Capric (1)	0.005	0.376	0.501	0.021	0.053	0.26	0.55	0.037	0.077	b
Lauric (2)	0.133	0.041	0.083	0.004	−0.011	0.36	0.59	0.005	0.013	b
Lauric (1)	0.004	0.467	0.687	0.021	0.040	2.45	5.73	0.048	0.081	b
Myristic (2)	0.067	0.036	0.068	0.005	−0.011	0.31	0.75	0.005	0.010	b
Myristic (1)	0.004	0.241	0.416	0.010	0.047	0.38	1.10	0.012	0.043	e
Palmitic (2)	0.067	0.031	−0.072	0.014	−0.045	0.34	0.68	0.009	0.026	a
Palmitic (1)	0.005	0.110	0.174	0.011	0.286	0.92	1.76	0.014	0.034	a
Stearic (2)	0.007	0.951	1.836	0.034	0.059	3.55	7.78	0.033	0.058	b

[a]Activity coefficient models: (a) UNIQUAC, (b) Wilson, (c) Margules, (d) NRTL, (e) van Laar.

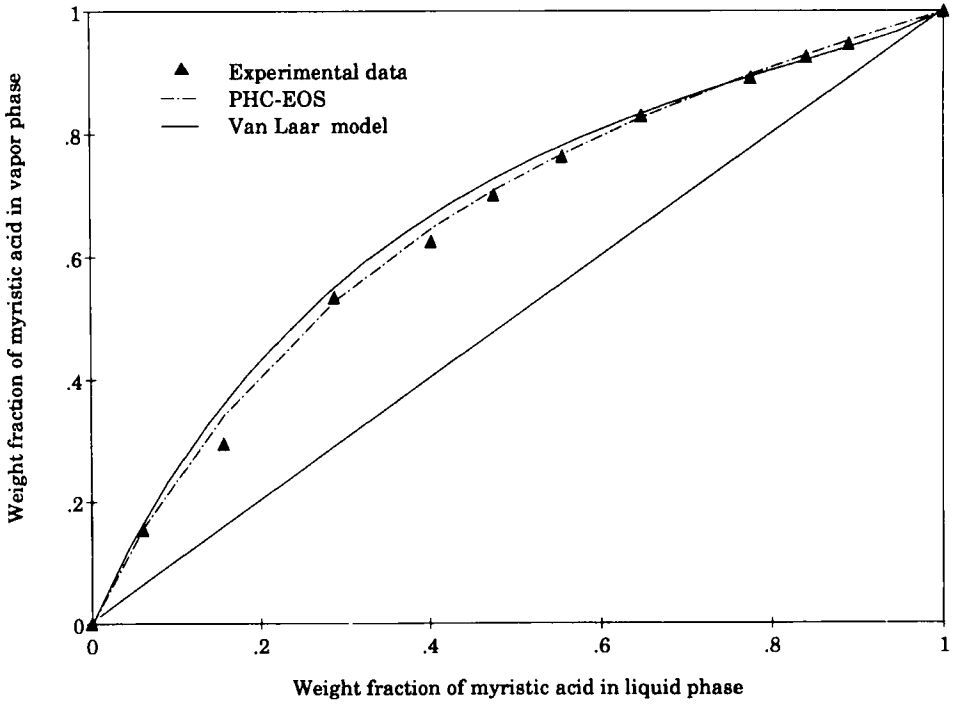

FIG. 4. Calculated and experimental VLE for myristic acid–palmitic acid system at 4 mbar.

(*30*). These results clearly indicate that the PHC-EOS reproduces binary VLE at very low pressures with the same degree of precision, if not better, as do models for activity coefficients. Furthermore, by being capable of calculating all thermodynamic properties needed, and accurately predicting VLE at both low and high pressures, using only one binary interaction parameter, PHC-EOS should be recommended for use in the simulation of distillation processes for the separation of fatty acids.

VLE of multicomponent systems must be known since separations of binary mixtures are rare in practice. The PHC-EOS is able to predict the behavior of multicomponent systems on the basis of binary interaction parameters, obtained from binary VLE data as outlined above.

The distillation process, shown in Fig. 2, was simulated using the *Aspen Plus* flow-sheeting program (*31*) and the PHC-EOS without dimerization equilibria. The fatty acid mixture was simulated as a 5-component system consisting of C_{14}–C_{20} fatty acids and water. Water was included since direct steam is injected in the reboilers of both columns and the feed cannot be completely dehydrated prior to distillation. The first column has 20 trays and is provided with a multitray feed configuration, a reboiler, and a partial

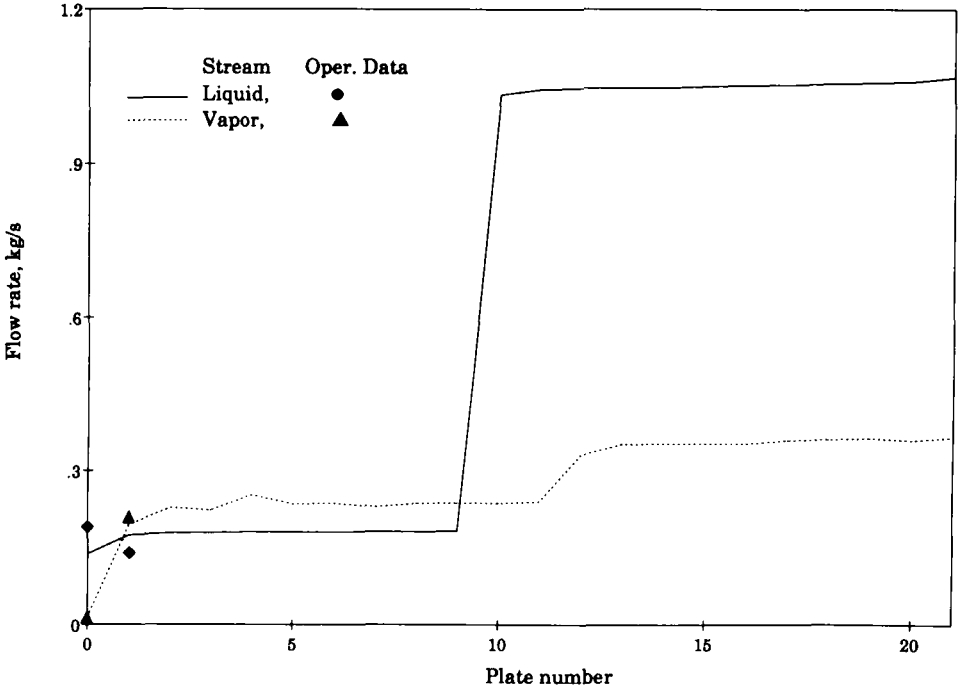

FIG. 5. Plant operating data and calculated flow rate profiles.

condenser. In our case the saturated feed is introduced on the 10th tray. The distillation still is equivalent to one tray and is provided with a reboiler and two partial condensers.

The simulation results for the distillation column are shown in Figs. 5–8, where the flow rate of both liquid and vapor streams, liquid- and vapor-phase composition, and temperature profiles are plotted as functions of the tray number in the column. Real operating data, measured from the plant of a major Swedish fatty acid producer, are also plotted for comparison. The plant capacity is 25,000 ton fatty acids/year with tallow being the main raw material used. Different fatty acid fractions can be produced with C_{16}–C_{18} mixtures being the major product. The comparison between simulated and measured data is very good for liquid-phase compositions, Fig. 6, and reasonably good for the flow rates, Fig. 5, and temperature, Fig. 8. It should be mentioned that the binary interaction parameters were set equal to zero for all binaries containing archidic acid. Furthermore, liquid compositions were analyzed using GC, while flow rate and temperature values were taken from the computerized data system of the plant.

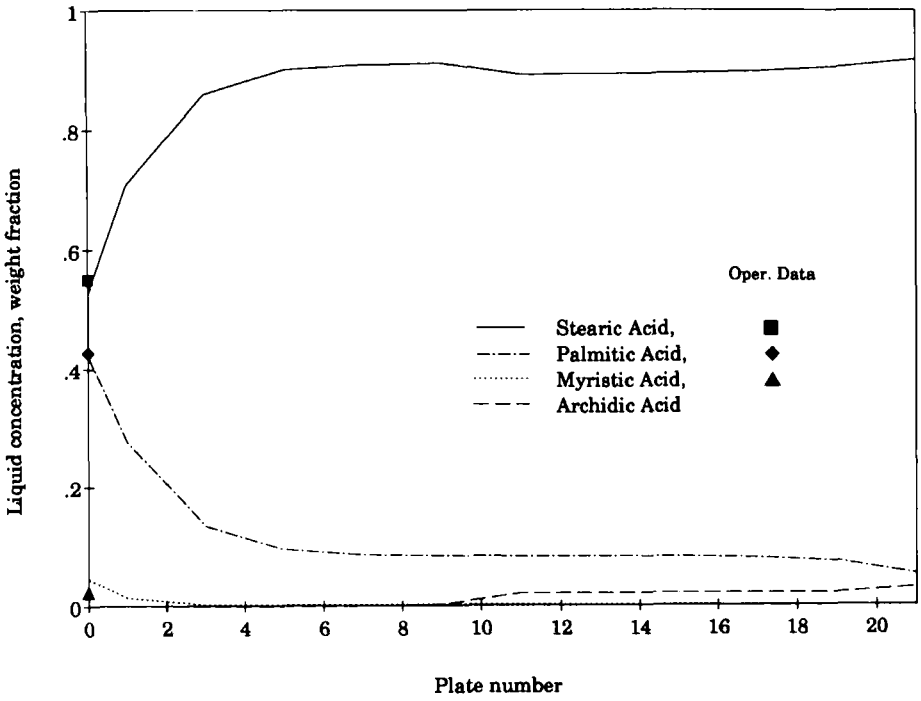

FIG. 6. Plant operating data and calculated liquid concentration profiles.

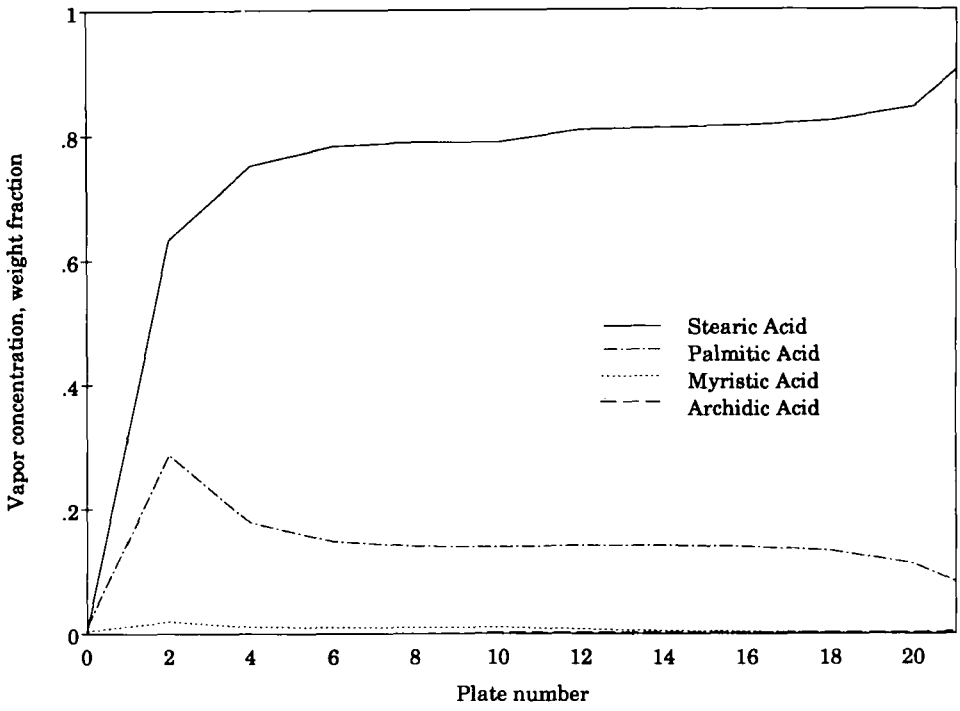

FIG. 7. Calculated vapor concentration profiles.

Higher accuracy in the measured liquid-phase compositions can therefore be anticipated compared to those for flow rates and temperatures. As mentioned earlier, the dimerization equilibria were not superimposed on the PHC-EOS model, a factor which also could explain the discrepancies between simulated and some plant operating data.

The simulation of the distillation still gave satisfactory results. Expressed in weight %, the normalized composition of the main product stream was measured as 3.80% C_{16}, 95.11% C_{18}, and 1.09% C_{20}. The simulated values for the same stream were 0.01% C_{14}, 5.70% C_{16}, 93.86%, C_{18}, 0.22% C_{20}, and 0.21% water.

In conclusion, the results obtained from the PHC-EOS are very good, especially in view of the fact that only one binary interaction parameter has been fitted to the binary vapor–liquid equilibrium data. Both thermodynamic and process simulations clearly indicated that this equation of state is very well suited for simulating different distillation processes used for the fractionation of different fatty acid feedstocks.

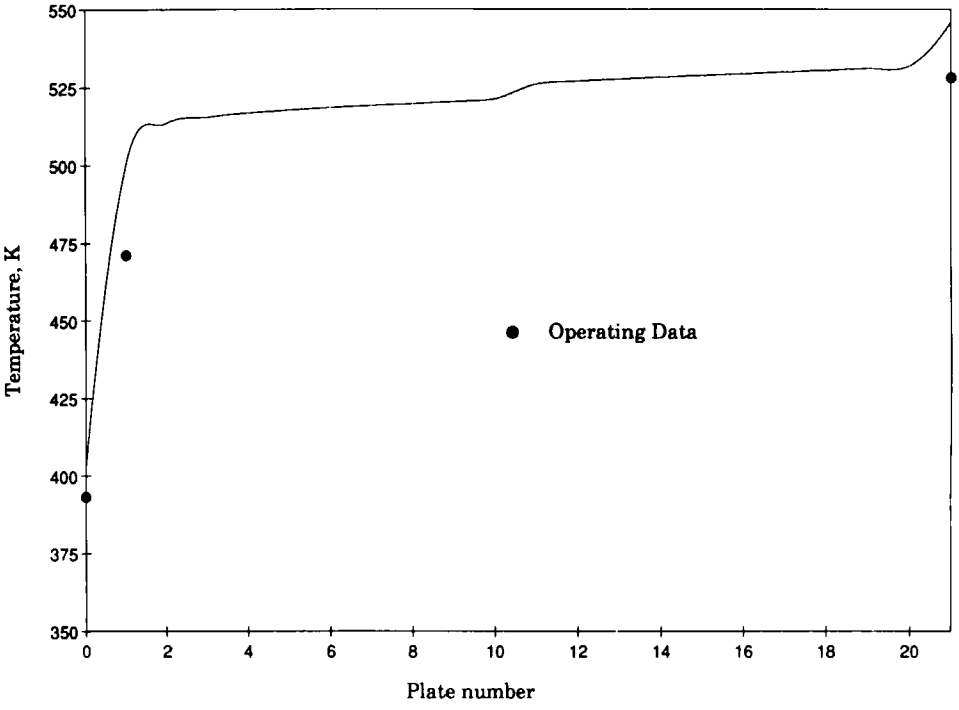

FIG. 8. Plant operating data and calculated temperature profile.

Acknowledgments

The authors are grateful to Mr. Stig Nydahl, Mr. Lars Pettersson, and Mr. Bengt Aberg of Karlshamns TEFAC AB, Sweden, for their cooperation, for supplying the necessary process data, and for their kind permission to publish the results.

SYMBOLS

A_{mn}	dimensionless constants used to calculate perturbations in compressibility factor
A, B, C	Antoine constants
c_i	Prigogine factor, defined as one-third the total number of external degrees of freedom per molecule i
Δh_i, Δh_{ij}	standard-state enthalpy of monomer and dimer species (J/kg·mol)
K_{ij}	self-dimerization equilibrium constant
k_{ij}	binary interaction parameter of the PHC-EOS
P	total pressure (bar)

P_c	critical pressure (bar)
P^s	vapor pressure of pure component (Pa)
R	gas constant (J/kg·mol·K)
Δs_{ij}	standard-state entropy of dimerization (J/kg·mol·K)
T	absolute temperature (K)
T_c	critical temperature (K)
T^*	characteristic temperature (K)
v	molar volume (L/mol)
v_c	critical volume (cm^3/mol)
v^*	hard-core molar volume (L/mol)
$\tilde{v}$	reduced molar volume
Z	compressibility factor
z_i, z_j, z_{ij}	true mole fraction of monomer and dimer species
ξ	reduced density
σ_{av}	percent of average relative deviation (%)
σ_{max}	percent of maximum relative deviation (%)
ϕ_i, ϕ_{ij}	true fugacity coefficient of monomer and dimer species
ω	acentric factor

REFERENCES

1. A. J. Kaufman and R. J. Ruebusch, *INFORM, 1*(12), 1034 (1990).
2. R. W. Johnson and E. Fritz (eds.), *Fatty Acids in Industry*, Dekker, New York, 1989.
3. H. Stage, *J. Am. Oil Chem. Soc., 61*, 204 (1984).
4. I. Ashour, Ph.D. Thesis, Lund University, Sweden, 1989.
5. K. P. Johnston, D. G. Peck, and S. Kim, *Ind. Eng. Chem., Res., 28*, 1115 (1989).
6. J. F. Brennecke and C. A. Eckert, *AIChE J., 35*, 1409 (1989).
7. P. M. Mathias, *Ind. Eng. Chem., Process Des. Dev., 22*, 385 (1983).
8. G. Soave, *Chem. Eng. Sci., 39*, 357 (1984).
9. R. M. Gibbons and A. P. Laughton, *J. Chem. Soc., Faraday Trans., 2*(80), 1019 (1984).
10. R. Stryjek and J. H. Vera, *Can. J. Chem. Eng., 64*, 323 (1986).
11. R. Stryjek and J. H. Vera, *Ibid., 64*, 334 (1986).
12. R. Stryjek and J. H. Vera, *ACS Symp. Ser., 300*, 560 (1986).
13. G. Wilczek-Vera and J. H. Vera, *Fluid Phase Equil., 37*, 241 (1987).
14. G. A. Melhem, R. Saini, and B. M. Goodwin, *Ibid., 47*, 189 (1989).
15. H. Orbey and J. H. Vera, *Chem. Eng. Sci., 45*, 3319 (1990).
16. H. Wogatzki and B. Gutsche, *Chem. Eng. Prog., 24*, 57 (1988).
17. D. Y. Peng and D. B. Robinson, *Ind. Eng. Chem., Fundam., 15*, 58 (1976).
18. G. Soave, *Chem. Eng. Sci., 27*, 1197 (1972).
19. Aa. Fredenslund, R. L. Jones, and J. M. Prausnitz, *AIChE J., 21*, 1086 (1975).
20. C. Tsonopoulos and J. M. Prausnitz, *Chem. Eng. J., 1*, 273 (1970).
21. L. V. Jasperson, L. C. Wilson, C. J. Brady, W. V. Wilding, and G. M. Wilson, *AIChE Symp. Ser., 85*(271), 102 (1989).
22. S. Beret and J. M. Prausnitz, *AIChE J., 21*, 1123 (1975).
23. M. D. Donohue and J. M. Prausnitz, *Ibid., 24*, 849 (1978).
24. J. Gmehling, D. D. Liu, and J. M. Prausnitz, *Chem. Eng. Sci., 34*, 951 (1979).
25. D. Ambrose and N. B. Ghiassee, *J. Chem. Thermodyn., 19*, 505 (1987).

26. R. C. Reid, J. M. Prausnitz, and T. K. Sherwood, *The Properties of Gases and Liquids*, 3rd ed., McGraw-Hill, New York, 1977.
27. I. Ashour and R. Wennersten, *J. Supercrit. Fluids*, *2*, 73 (1989).
28. D. S. Abrams, H. A. Massaldi, and J. M. Prausnitz, *Ind. Eng. Chem., Fundam.*, *13*, 259 (1974).
29. J. Gmehling, U. Onken, and P. Grenzheuser, *Vapor–Liquid Data Collection*, Vol. I, Part 5, Dechema, Frankfurt am Main, 1982.
30. G. Aly and G. Zacchi, *Report LUTKDH/(TKKA-3003)/1-38/(1979)*, Department of Chemical Engineering I, Lund Institute of Technology, 1979.
31. *Aspen Plus*, Aspen Technology, Inc., Cambridge, Massachusetts.

Received by editor July 15, 1991